Trans Indian Inst Met (2015) 68(6):1221–1226
DOI 10.1007/s12666-015-0709-3

TECHNICAL PAPER

Phase Evolution in Hypereutectic $Al_{90}Cu_{10-x}Ni_x$ (x = 0, 5) Alloys

Sumanta Samal[1] · **Gandham Phanikumar**[1]

Received: 29 June 2015 / Accepted: 8 September 2015 / Published online: 12 October 2015

Abstract The present work is aimed at understanding the phase evolution of hypereutectic Al-rich Al–Cu–Ni in situ composites consisting of ultrafine eutectic with micron scale dendrites. The hypereutectic $Al_{90}Cu_{10-x}Ni_x$ (x = 0, 5) are synthesized by vacuum arc melting technique under high purity argon atmosphere. Detailed X-ray diffraction and electron microscopic (SEM and TEM coupled with EDS) studies have been carried out to identify the phases in these alloys. Thermodynamic calculations performed using CALPHAD approach using ThermoCalc® software predict the equilibrium solidification path. The $Al_{90}Cu_5Ni_5$ alloy exhibits ternary quasi-peritectic reaction of $L + Al_3Ni \rightarrow (Al)_{ss} + Al_3Ni_2$ at invariant point, which is supported by two univariant reactions i.e. $L + Al_3Ni \rightarrow Al_3Ni_2$ and $L \rightarrow (Al)_{ss} + Al_3Ni_2$ above and below the invariant point respectively.

Keywords Aluminium alloys · Microstructure · Quasi-peritectic reaction · X-ray diffraction · Electron microscopy

1 Introduction

Al-based alloys have been researched extensively in the last few decades due to their high specific strength, good formability, excellent corrosion resistance etc. and are considered as preferred alloys for structural applications in the aerospace and automotive industries [1–3]. However, there is an increasing demand for novel Al-based alloys with a good combination of strength and ductility. There have been efforts to develop novel Al-based alloys with improved mechanical properties both at room and elevated temperature [4–6]. He et al. [7] have reported for the first time the novel Ti-based in situ composites such as Ti–Cu–Ni–Sn–Nb/Ta [7–9], consisting of nano/ultrafine eutectic matrix and micron-sized primary dendrite. Thereafter, large number of investigations on the in situ composites such as Ti–Fe–Sn [10–14], Ti–Fe–Co [15–18], Ti–Cu–Ni–Sn–Nb/Ta [7–9], Ti–Ta–Ni–Cu–Co [19] has been reported in the literature.

Since microstructure plays a significant role in achieving improved mechanical properties, it is necessary to understand the phase evolution in a newly designed multicomponent alloy. In the present investigation, an Al-rich nano-/ultrafine in situ composite is designed and studied to understand the phase evolution with an intended use at high temperature. Al-based multicomponent alloys have been designed by choosing Al–Cu as base binary alloy system. Al–Cu based alloys can be further strengthened with trace additions of a third element such as Ni, Si, Mn etc. which can be considered as suitable candidates for moderate-temperature as well as high-strength applications in the aerospace industry because of their excellent thermal stability [20].

In the Al-rich side of the Al–Cu phase diagram [21] (Fig. 1a), there is a eutectic reaction i.e. $L \rightarrow (Al)_{ss} + Al_2Cu$ at 548.2 °C. Due to the addition of Ni as alloying element in Al, there is a possibility of formation of Al_3Ni and Al_3Ni_2 phases in the Al-rich side of Al-Ni phase diagram (Fig. 1b). Al_3Ni phase is formed by means of two pathways i.e. (1) by peritectic reaction i.e. $L + Al_3Ni_2 \rightarrow Al_3Ni$ at 854 °C and (2) eutectic reaction i.e.

✉ Gandham Phanikumar
gphani@iitm.ac.in

[1] Department of Metallurgical and Materials Engineering, Indian Institute of Technology Madras, Chennai, Tamil Nadu 600036, India

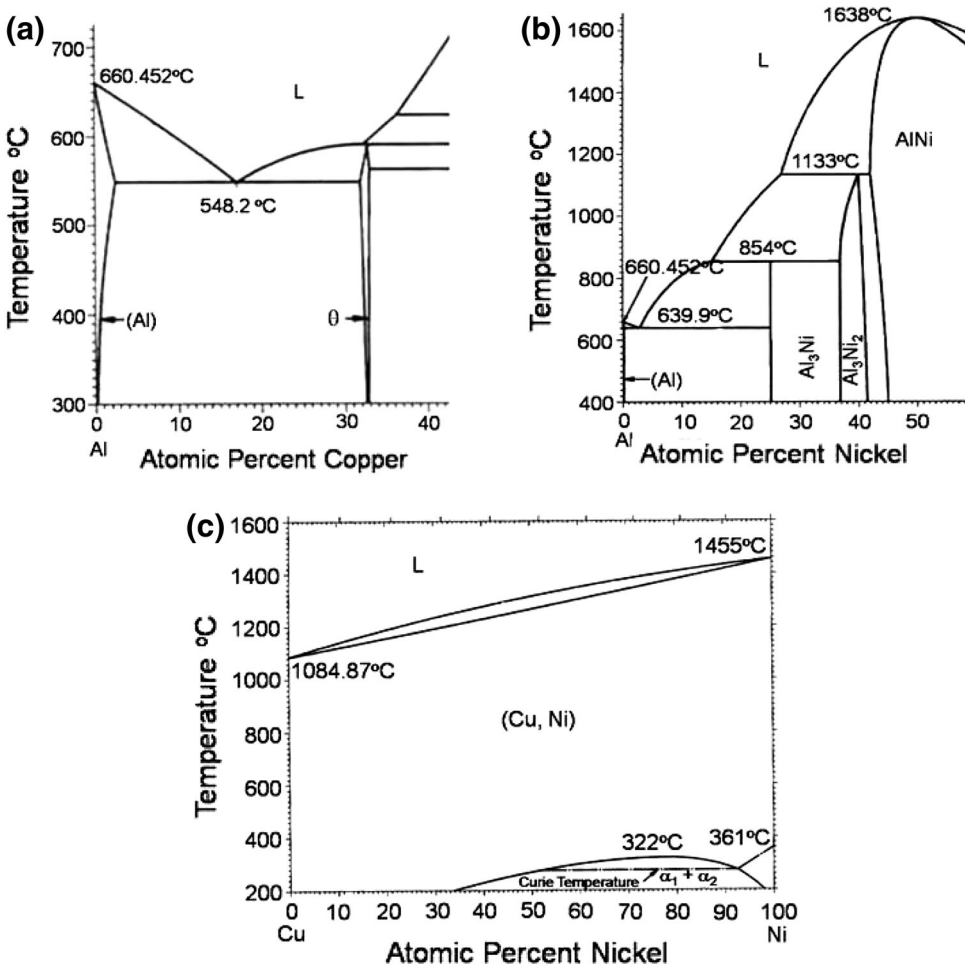

Fig. 1 Phase diagrams of **a** Al–Cu, **b** Al–Ni and **c** Cu–Ni systems [21]

$L \rightarrow (Al)_{ss} + Al_3Ni$ at 639.9 °C. It is found that Ni is soluble in Cu in the entire composition range (Fig. 1c). These possibilities from the respective binary phase diagrams has aided the development of the multi-component alloy chosen for this study.

2 Experimental

High purity commercial Al, Cu and Ni (≥99.9 %) were used as the starting materials. Ternary Al–Cu–Ni alloys were prepared by arc melting under ultra-high purity argon gas on a water cooled copper hearth to obtain arc melted alloy buttons. These alloys were repeatedly melted about 5–6 times to ensure chemical homogeneity. The phase identification of as-cast alloys was examined by X-ray diffraction (XRD) (Analytical X-pert pro instrument) with Cu K_α ($\lambda = 0.154056$ nm) radiation, operating at 45 kV and 30 mA, with step size of $2\theta = 0.017$ °. The peaks in the diffraction patterns were identified using International Committee for Diffraction Data (ICDD) database. The phase distribution and compositional analyses on the polished section of the as-cast samples were observed using the scanning electron microscope equipped with an energy-dispersive spectrometer (EDS).Micrographs were obtained in the back scattered electron (BSE) imaging mode to reveal the different phases in the microstructure by the atomic number (Z) contrast. In addition, the composition of different phases in the microstructure had been measured by using energy dispersive X-ray spectroscopic (EDS) analysis. Fine scale microstructural observations were carried out using FEI Tecnai G^2 U-Twin TEM, operated at 200 kV.

3 Results

3.1 X-Ray Diffraction (XRD)

The XRD patterns of the as-cast $Al_{90}Cu_{10-x}Ni_x$ ($x = 0$, 5 atom%) alloys are shown in Fig. 2. The pattern for $Al_{90}Cu_{10}$ alloy reveals the presence of fcc $(Al)_{ss}$ ($Fm\bar{3}m$, $a = 0.40494$ nm) and tetragonal Al_2Cu ($I4/mcm$, $a = 0.60654$ nm and $c = 0.48734$ nm) phases. While fcc $(Al)_{ss}$, orthorhombic Al_3Ni (Pnma, $a = 0.6598$ nm,

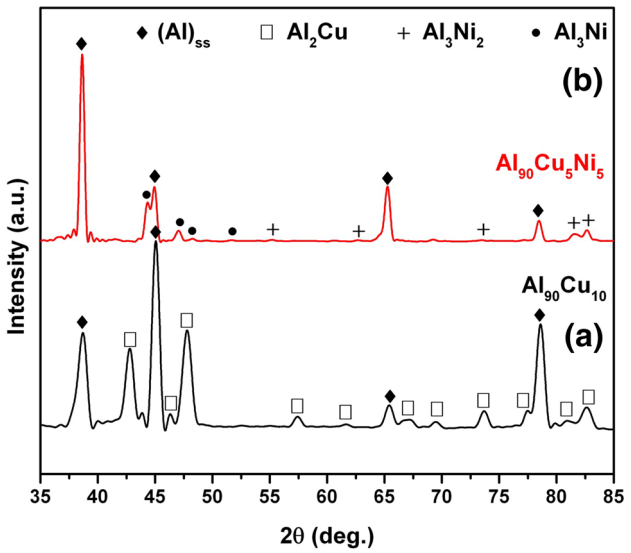

Fig. 2 XRD pattern of (*a*) $Al_{90}Cu_{10}$ and (*b*) $Al_{90}Cu_5Ni_5$ alloys

b = 7352 nm, c = 0.4802 nm) and hexagonal Al_3Ni_2 ($P\bar{3}m1$, a = 0.4028 nm and c = 0.4891 nm) phases have also been observed in the XRD pattern of $Al_{90}Cu_5Ni_5$ alloy.

3.2 Scanning Electron Microscopic (SEM) Observation

The detailed SEM characterization of all the as-cast alloys have been carried out. However, representative SEM micrographs of the alloys have been shown to elucidate the phase formation in the different alloy compositions. The different phases in the microstructure are marked based on the compositional measurements. For the hypereutectic $Al_{90}Cu_{10}$ binary alloy (Fig. 3a), the microstructure consists of eutectic between Al_2Cu and $(Al)_{ss}$ along with micron-sized $(Al)_{ss}$ (dark contrast) dendrites. While the SEM micrograph of $Al_{90}Cu_5Ni_5$alloy is shown in Fig. 3b, which reveals the presence of different kinds of dendrites i.e. $(Al)_{ss}$ (dark contrast), Al_3Ni_2 (bright contrast) and Al_3Ni (gray contrast) phases along with eutectic between Al_3Ni_2 and $(Al)_{ss}$ phases. The microstructure clearly reveals the signature of an incipient peritectic reaction, leading to the formation of the Al_3Ni_2 phase i.e. Al_3Ni_2 phase is formed due to the peritectic reaction between the liquid and Al_3Ni phase ($L + Al_3Ni \rightarrow Al_3Ni_2$). The typical capped morphology is a signature of the peritectic reaction [22].

3.3 Transmission Electron Microscopic (TEM) Observation

The SEM observations of the investigated Al–Cu–Ni alloys have further been confirmed by TEM studies. The detailed

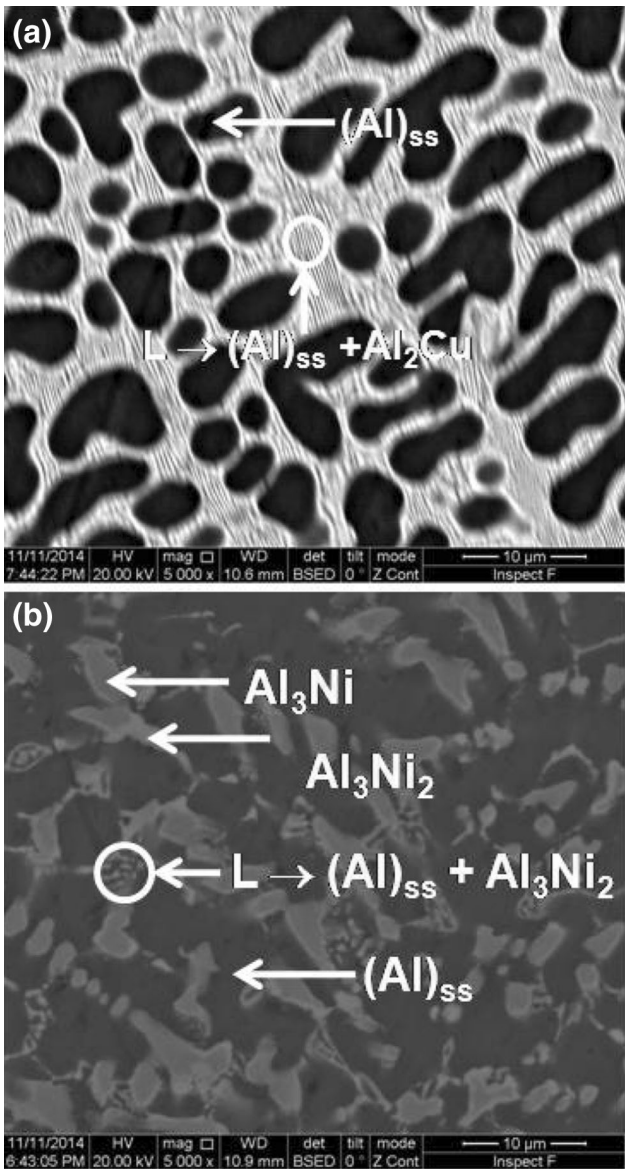

Fig. 3 BSE-SEM micrograph of **a** $Al_{90}Cu_{10}$ and **b** $Al_{90}Cu_5Ni_5$ alloys

TEM investigation of the as-cast $Al_{95}Cu_5Ni_5$ alloy has been carried out to determine the phases present in the microstructure as well as to infer different phase equilibria and phase transformations that occurred during solidification of this alloy. In this paper, only a few representative microstructures are presented. The constituent phases in the microstructure are identified by energy dispersive spectroscopy (EDS) analysis. The characteristic bright field micrograph of as-cast $Al_{95}Cu_5Ni_5$ alloy is shown in Fig. 4, revealing the presence of eutectic microstructure along with dendritic phases. The eutectic consists of Al_3Ni_2 and $(Al)_{ss}$ phases (Fig. 4b). The microstructure also displays two other dendritic phases i.e. $Al_3Ni$and Al_3Ni_2 (Fig. 4a).

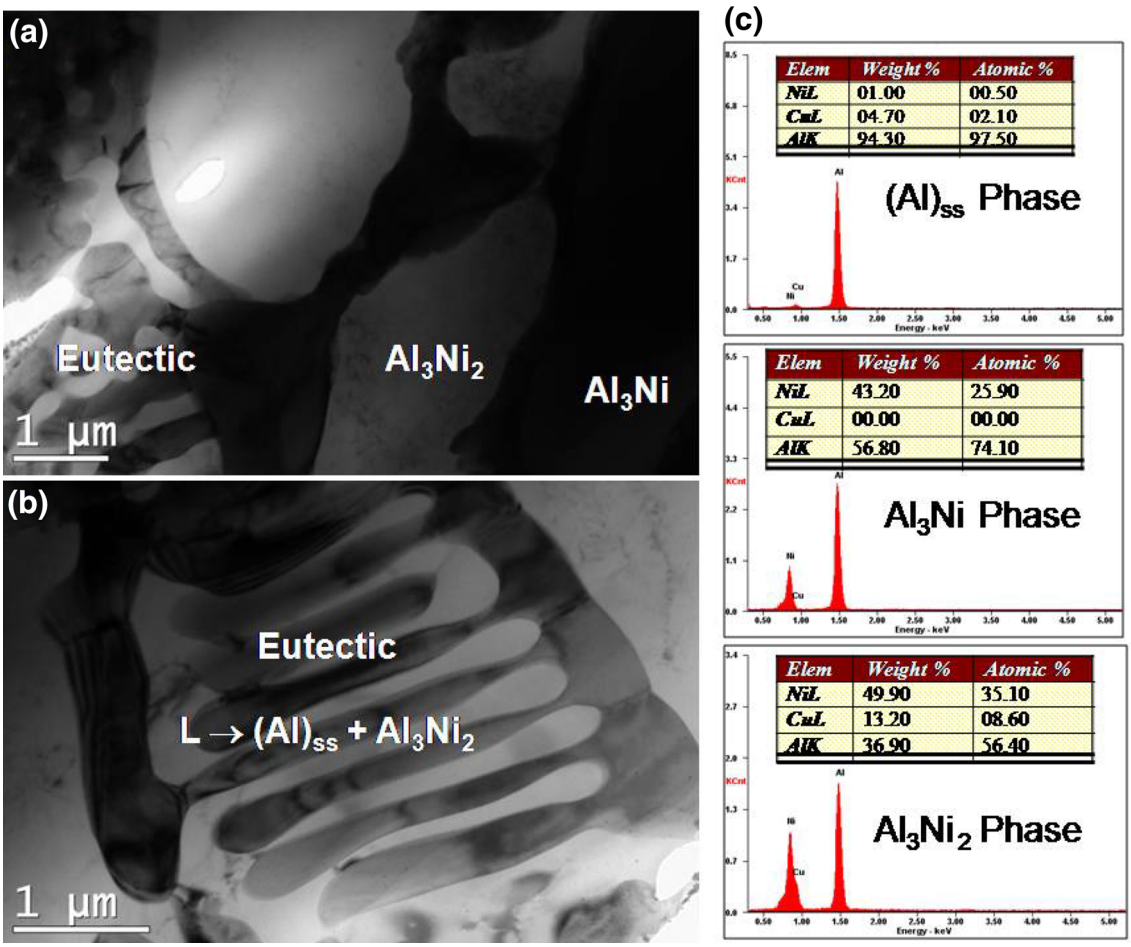

Fig. 4 **a** Bright field TEM micrograph of $Al_{90}Cu_5Ni_5$ alloy showing eutectic region, Al_3Ni_2 and Al_3Ni phases. **b** Bright field TEM micrograph of $Al_{90}Cu_5Ni_5$ alloy showing the eutectic to be comprising of $(Al)_{ss}$ and Al_3Ni_2 phases. **c** EDS patterns of $(Al)_{ss}$, Al_3Ni and Al_3Ni_2 phases taken at the regions in the corresponding micrographs in **a** and **b**

3.4 Thermodynamic Simulations on Solidification Path

The thermodynamic simulations have been carried out to predict the equilibrium solidification path using the CALPHAD approach using ThermoCalc® software and TCAL2® database. The solidification path observed in most industrial processes deviates from the equilibrium one due to solute segregation. Scheil model has been adopted here to describe the solute redistribution during solidification. This model assumes complete diffusion in liquid, but no diffusion in solid and local equilibrium at the interface [23]. Diffusion of solute in the solid is often limited, especially in the case of substitutional solid solution with large atomic size and hence Scheil model is considered to be more appropriate to predict the real solidification qualitatively. The pseudo-binary phase diagrams of the studied hypereutectic $Al_{90}Cu_{10-x}Ni_x$ (x = 0, 5) alloys were calculated, as shown in Fig. 5. The equilibrium solidification path for the $Al_{90}Cu_{10}$ alloy (Fig. 5a) can be described as:

$$L \rightarrow FCC\_L12 + L \rightarrow AL2CU\_C16 + FCC\_L12 + L \rightarrow AL2CU\_C16 + FCC\_L12$$

i.e.

$$L \rightarrow (Al)_{ss} + L \rightarrow Al_2Cu + (Al)_{ss} + L \rightarrow Al_2Cu + (Al)_{ss}.$$

This means that first, primary $(Al)_{ss}$ phase is formed in the liquid and finally the liquid transforms into a mixture of $(Al)_{ss}$ and Al_2Cu phases. While the equilibrium solidification path for $Al_{90}Cu_5Ni_5$ alloy (Fig. 5b) can be described as:

$$L \rightarrow FCC\_L12 + L \rightarrow BCC\_B2 + FCC\_L12 + L \rightarrow AL7CU4NI + BCC\_B2 + FCC\_L12 + L \rightarrow AL7CU4NI + BCC\_B2 + FCC\_L12$$

i.e.

$$L \rightarrow (Al)_{ss} + L \rightarrow AlNi + (Al)_{ss} + L \rightarrow Al_7Cu_4Ni + AlNi + (Al)_{ss} + L \rightarrow Al_7Cu_4Ni + AlNi + (Al)_{ss}.$$

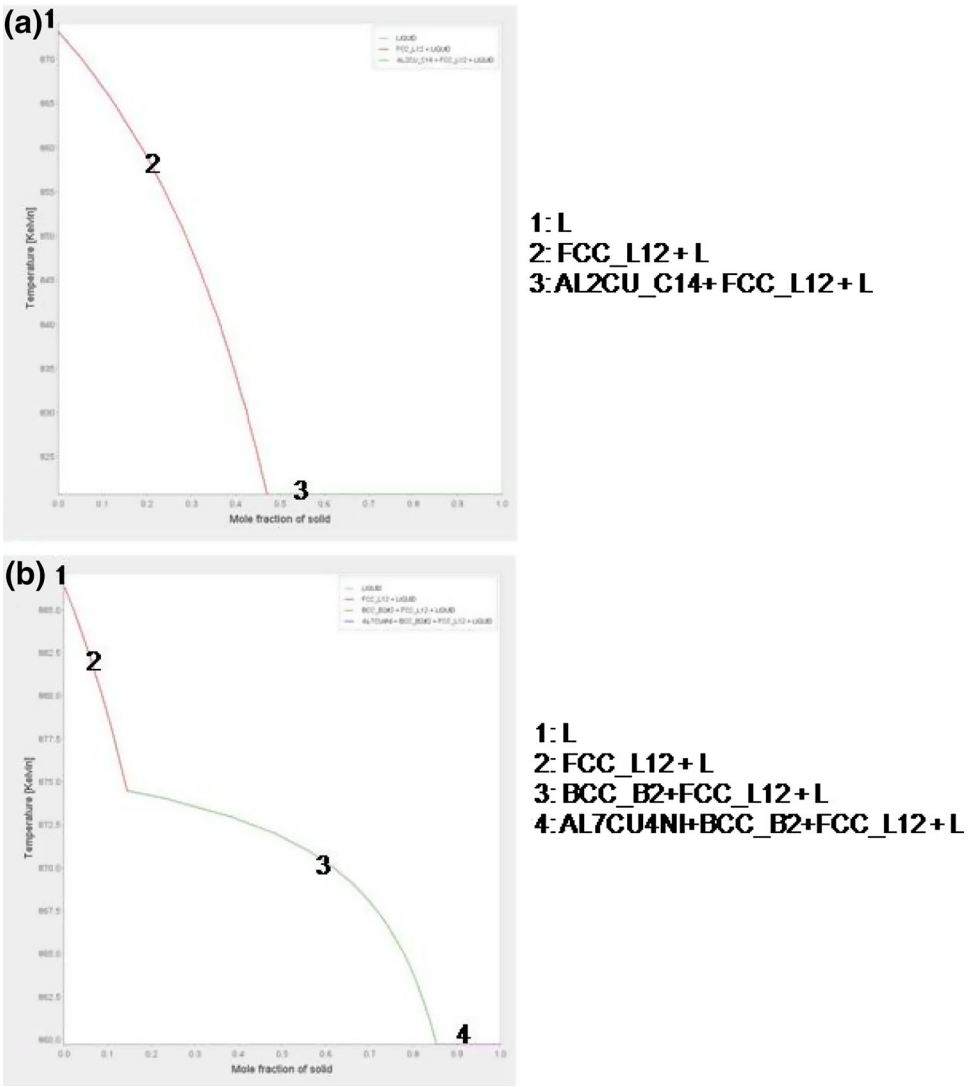

Fig. 5 Plot between the mole fraction of solid versus temperature for the studied alloy using Scheil model **a** $Al_{90}Cu_{10}$ and **b** $Al_{90}Cu_5Ni_5$ alloys

This means that first, primary $(Al)_{ss}$ phase is formed in the liquid followed by secondary AlNi phase and then a small amount of Al_7Cu_4Ni is evolved during last stage of solidification. Finally, the liquid transforms into a mixture of $(Al)_{ss}$, AlNi and Al_7Cu_4Ni phases.

4 Discussion

For the binary $Al_{90}Fe_{10}$ alloy, the primary dendritic phase, $(Al)_{ss}$ is formed first from the liquid ($L \rightarrow L + (Al)_{ss}$) during solidification. Thereafter, the remaining liquid undergoes eutectic reaction to form Al_2Cu and $(Al)_{ss}$ ($L \rightarrow Al_2Cu + (Al)_{ss}$) which is in accordance with the equilibrium phase diagram [21]. For $Al_{90}Cu_5Ni_5$ alloy, at first Al_3Ni primary dendrite is formed i.e. $L \rightarrow L + Al_3Ni$. Subsequently, the Al_3Ni_2 phase is evolved due to peritectic reaction between the liquid and Al_3Ni phase. Finally, the remaining liquid undergoes eutectic reaction leading to the formation of $(Al)_{ss}$ and Al_3Ni_2 phases i.e. $L \rightarrow (Al)_{ss} + Al_3Ni_2$. It is also observed from microstructural features (Fig. 3b) that there is a clear signature of ternary four phase equilibrium reaction, which is coupled with two monovariant reactions i.e. one peritectic reaction ($L + Al_3Ni \rightarrow Al_3Ni_2$) and other one is eutectic reaction ($L \rightarrow (Al)_{ss} + Al_3Ni_2$). Therefore the actual solidification path ways for $Al_{90}Cu_5Ni_5$ alloy can be described as follows. At first the primary Al_3Ni dendrite is formed from the liquid, followed by the formation Al_3Ni_2 phase via univariant reaction ($L + Al_3Ni \rightarrow Al_3Ni_2$). Thereafter, the composition of the remaining melts changes and hence moves towards the invariant ternary quasi-peritectic point. At invariant point, the four phase equilibrium

reaction i.e. $L + Al_3Ni \rightarrow (Al)_{ss} + Al_3Ni_2$ occurs. Then the $(Al)_{ss}$ and Al_3Ni_2 phases are precipitated from the remaining melt and proceeds along the other monovariant line separating $(Al)_{ss}$ and Al_3Ni_2 phase fields. It is to be noted that the phase evolution in $Al_{90}Cu_{10}$ binary alloys, predicted by Scheil model is similar to the experimental results, whereas in case of $Al_{90}Cu_5Ni_5$ ternary alloy, there is disagreement with the experimental results. There are significant discrepancies between the calculated results using Scheil model and experimental results in $Al_{90}Cu_5Ni_5$ alloy because of the solid state diffusion of solute during peritectic transformation being not considered in Scheil model. The $Al_{90}Cu_5Ni_5$ ternary alloy exhibits ternary four phase equilibrium reaction. This type of reaction has been observed in several ternary systems such as steels (Fe–Cr–Ni alloy), Ti-alloys (Ti–Fe–Sn, Ti–Fe–Co), Al-alloys (Al–Cu–Fe) etc. [22], which are technologically important. Thus, Al–Cu–Ni alloys exhibiting ternary four phase equilibrium reaction open up new possibilities for a novel microstructure design.

5 Conclusions

The $Al_{90}Cu_5Ni_5$ alloy exhibits ternary quasi-peritectic reaction of $L + Al_3Ni \rightarrow (Al)_{ss} + Al_3Ni_2$ at invariant point. The proposed ternary quasi-peritectic reaction is cooperated by the two univariant reactions i.e. $L + Al_3Ni \rightarrow Al_3Ni_2$and $L \rightarrow (Al)_{ss} + Al_3Ni_2$ above and below the invariant point, respectively. The solidification path for the ternary alloys deviates from the Scheil simulated path.

Acknowledgments One of the authors (S.S.) wishes to thank IIT Madras for the post-doctoral fellowship that has made this study possible. The authors also thank Dr. K. Biswas (IIT Kanpur) for his support in some of the research facilities.

References

1. ASM Handbook, *Properties and Selection: Nonferrous Alloys and Special-Purpose Materials*, Materials Park, Ohio, US (1990).
2. Li Y, Georgarakis K, Pang S, Antonowicz J, Charlot F, Lemoulec A, Zhang T, and Yavari A R, *J Alloys Compd* **447** (2009) 346.
3. Sun B A, Pan M X, Zhao D Q, Wang W H, Xi X K, Sandor M T, and Wu Y, *Scr Mater* **59** (2008) 1159.
4. Mondal C, Mukhopadhyay A K, Raghu T, and Varma V K, *Mater Sci Eng A* **454** (2007) 673.
5. Mondal C, Singh A K, Mukhopadhyay A K and Chattopadhyay K, *Mater Sci Eng A* **577** (2013) 87.
6. Nandi P, Suwas S, Kumar S, and Chattopadhyay K, *Metall Mater Trans A* **44** (2013) 2591.
7. He G, Eckert J, Löser W, and Schultz L, *Nat Mater* **2** (2003) 33.
8. He G, Löser W, and J. Eckert, *Acta Mater* **51** (2003) 5223.
9. He G, Eckert J, Löser W, and Hagiwara M, *Acta Mater* **52** (2004) 3035.
10. Zhang L C, Das J, Lu H B, Duhamel C, Calina M, and Eckert J, *Scr Mater* **57** (2007), 101.
11. Das J, Kim K B, Baier F, Löser W, Gebert A, and Eckert J, *J Alloys Compd* **434–435** (2007) 28.
12. Das J, Kim K B, Xu W, Löser W, and Eckert J, *Mater Sci Eng A* **449–451** (2007) 737.
13. Samal S, Mondal B, Biswas K, and Govind, *Metall Mater Trans A* **44** (2013) 427.
14. Mondal B, Samal S, Biswas K and Govind, *IOP Conf Series: Mater Sci Eng* **27** (2011) 012025.
15. Louzguine D V, Kato H, and Inoue A, *Philos Mag Lett* **84** (2004) 359.
16. Louzguine-Luzgin D V, Louzguina-Luzgina L V, Kato H, and Inoue A, *Acta Mater* **53** (2005) 2009.
17. Samal S, Gautam P, Agarwal S, and Biswas K, *Mater Sci Forum* **790** (2014) 497.
18. Samal S, Gautam P, Agarwal S, and Biswas K, *Metall Mater Trans A* **46** (2015) 851.
19. Samal S, and Biswas K, *J Nanopart Res* **15** (2013).
20. Ünlü N, Gable B M, Shiflet G J, and Starke E A, *Metall Mater Trans* A **34** (2003) 2757.
21. Massalski T B, *Binary Alloy Phase Diagrams*, Second Edition, ASM International, Metals Park, OH, USA (1990).
22. Biswas K, and Samal S, in *Solidification of Containerless Undercooled Melts*, First Edition, (ed) Herlach D M, and Matson D M, WILEY VCH (2012).
23. Dantzig J A, and Rappaz M, *Solidification*, EPFL Press, Lausanne, Switzerland (2009).